J Mater Sci (2018) 53:3149–3162

Biomaterials

Photodegradation pathway of rhodamine B with novel Au nanorods @ ZnO microspheres driven by visible light irradiation

Ying Zhang[1], Jiabin Zhou[1,*], Zhen Li[1], and Qinqin Feng[1]

[1] School of Resources and Environmental Engineering, Wuhan University of Technology, 122 Luoshi Road, Wuhan 430070, China

Received: 31 August 2017
Accepted: 30 October 2017
Published online: 7 November 2017

ABSTRACT

A series of Au–ZnO photocatalysts were successfully synthesized from ZnO microspheres impregnated with Au nanorods by the seed-mediated method, and their photocatalytic activity of degradation of rhodamine B (RhB) was investigated. The nanocomposite catalyst exhibited high photocatalytic activity and degraded 92% of RhB solution under visible light irradiation in 330 min. The enhancement of photocatalytic effects was mainly ascribed to the surface plasmon resonance effect of Au nanorods; therefore, Au–ZnO spheres can absorb resonant photons and transfer the electron to the conduction band (CB) of ZnO leading to the separation of electrons and holes under visible light. Meanwhile, the photocatalytic performance was beneficial from the flower-like porous structure of ZnO, which enhances adsorption of the dye molecules and dissolved oxygen on the catalyst surface and facilitates the electron/hole transfer. Furthermore, the degradation pathway was proposed on the basis of the intermediates during the photodegradation process using liquid chromatography analysis coupled with mass spectroscopy (LC–MS). The degradation mechanism of pollutant is ascribed to the superoxide radicals ($\cdot O^{2-}$), which is the main oxidative species for the *N*-deethylated degradation of RhB. Moreover, the Au–ZnO photocatalysts demonstrated excellent photostability after five cycles. This work provides a facile and effective approach for removal of organic dyes under visible light and thus can be potentially used in the environmental purification.

Introduction

Semiconductor photocatalysis has attracted considerable research attention due to its great potential in addressing environmental remediation and energy conversion upon light absorption [1]. Up to date, a large variety of semiconductor photocatalysts (e.g., TiO_2 [2, 3], ZnO [4], Fe_2O_3 [5], Bi_2O_3 [6], g-C_3N_4 [7]) have been explored aiming at increased quantum efficiency, enhanced response to visible light

Address correspondence to E-mail: jbzhou@whut.edu.cn

https://doi.org/10.1007/s10853-017-1779-x

radiation and higher photochemical stability. Among these photocatalysts, ZnO has been extensively studied due to its efficient photocatalytic ability as well as nontoxic, low cost and good stability [8]. However, as one of the most efficient photocatalysts ZnO still has many drawbacks. One of the critical drawbacks of ZnO is that the wide band gap (~ 3.37 eV) makes it unable to efficiently utilize visible light [9]. Another drawback of ZnO is its fast recombination rate of the photogenerated electron–holes pairs in photocatalytic reactions, thus leading to decreased photocatalytic activity [10]. As a result, many methods have been used to improve the visible light utilization capability of ZnO, such as coupling with other semiconductors [11, 12], doping with nitrogen [13, 14], modification with carbon structures [15–17], doping with metal [18, 19] and noble metal [20–22]. Among these methods, Au nanoparticle doping has shown significant promise in visible light utilization in the photocatalytic process due to the surface plasmon resonance (SPR) effect. As one of the surface-sensitive techniques and commonly employed in chemical [23] and biological sensors [24], SPR effect is a coherent collective oscillation of electrons in the conduction band (CB) induces large surface electric fields that greatly enhance the irradiative properties of noble metal when they interact with resonant electromagnetic radiation [20]. After doping with Au nanoparticles, Schottky barriers are formed at the Au/ZnO junctions interface and Au nanoparticles act as electron trappers leading to the separation of electrons and holes [25] and thus greatly enhance the absorption and utilization of visible light.

Recent studies have shown that the shape of Au nanoparticles is an important parameter in governing their physical and chemical properties [20, 23, 26]. By adjusting the dimension of Au nanoparticles to Au nanorods, it is not only possible to tune the absorption wavelength from visible region to NIR region, but also to increase their absorption and scattering cross sections, thereby improving the utilization efficiency of the visible light [27]. In addition, ZnO has the richest morphologies, which are very complex and diversified and can be easily manipulated with a desirable structure [28]; therefore, researches have been rapidly progressing to modify the surface electronic structure of ZnO to inhibit charge recombination, such as providing a suitable geometric structure for effective carrier transfer pathways and exposing polar and nonpolar facts [28–36].

Herein, in this study a novel facile approach was adopted to fabricate Au nanorods @ flower-like ZnO microspheres (Au–ZnO) to tremendously accelerate the degradation rate of RhB under visible light. On the one hand, the Au nanorods act as effective antennas for visible light and lead to the promotion of photogenerated electrons by SPR. On the other hand, the flower-like morphological structure of ZnO largely increases the absorption efficiency of photons compared to normal ZnO nanoparticles. The composites showed significant enhanced photocatalytic activity in RhB degradation; moreover, the mechanism of RhB was also investigated.

Materials and methods

Materials

Zinc acetate, sodium citrate, sodium hydroxide, gold(III) chloride trihydrate ($HAuCl_4{\cdot}3H_2O$) (99.9%), sodium borohydride, ($NaBH_4$) (99.99%), mercaptopropionic acid (MPA) (99%), cetyltrimethyl ammonium bromide (CTAB), ascorbic acid (AA) (99%), silver nitrate ($AgNO_3$) (99.9%), ethanol, isopropanol and rhodamine B were all obtained from Sinopharm Co., Ltd. (China) and used without any further purification.

Sample preparation

Synthesis of flower-like ZnO microspheres

Flower-like ZnO microspheres were fabricated by a hydrothermal method. The preparation processes were as followed: 0.8299 g $C_4H_6O_4Zn{\cdot}2H_2O$ and 1.1029 g sodium citrate were dissolved into 60 mL deionized water with a ultrasonication lasting 5 min followed by a continuous stirring until a clear aqueous solution was obtained. Then, 6 mL of NaOH with concentration of 4.0 M was added into the prepared aqueous solution stirring for about 30 min to obtain white colloidal solutions. The mixture was then transferred to a Teflon-lined stainless steel reactor and heated at 120 °C for 8 h. After that, the colloids were centrifuged and further washed with alcohol and deionized water for several times before drying at 60 °C for 2 h. To compare with flower-like ZnO

microspheres, normal ZnO particles were fabricated by the same method without sodium citrate and were named as ZnO-n.

Synthesis of Au nanorods

The preparation of gold nanorods refers to the preparation method of Tapan K. Sau and Catherine J. Murphy [37].

Preparation of Au seeds Typically, 1.1 mL of an aqueous 1 g/L solution of $HAuCl_4$ was added to 10 mL of a 0.1 M CTAB solution in a test tube (plastic). Then, 0.6 mL of an aqueous 0.01 M ice-cold $NaBH_4$ solution was added. The obtained solution was kept undisturbed at 30 °C for at least 2 h.

Preparation of Au nanorods 5 mL of 0.2 M CTAB solution was added into 2 mL of 1 g/L $HAuCl_4$ solution. Then, 80 μL of 0.01 M $AgNO_3$ solution and 70 μL of 0.1 M ascorbic acid (AA) were added into the mixture solution. And then 60 μL of the as-prepared seed solution was added into the aforesaid solution. The obtained solution was kept undisturbed at 30 °C for at least 10 h. After that, the Au nanorod solution was centrifuged and further washed with deionized water for several times to remove CTAB.

Synthesis of Au nanorods @ flower-like ZnO microspheres

Mercaptopropionic acid (MPA) was used as bridge molecules to Au and ZnO. 200 mg of flower-like ZnO microspheres was added into 0.1 M MPA solution with rigorous stirring for about 30 min and then left undisturbed for 24 h at room temperature. After that, the excess MPA was washed with deionized water. A certain amount of Au nanorods were added into MPA-ZnO solution, respectively, with rigorous stirring for about 1 h, and then, the mixture solution was washed with deionized water. After that, the colloidal was dried at 80 °C for 4 h. The different concentrations of Au-modified ZnO were named as Au–ZnO-0.1, Au–ZnO-0.5, Au–ZnO-1, Au–ZnO-2, Au–ZnO-3 and Au–ZnO-4 (Au percentage concentration is shown in Table 1). In order to compare with Au nanorods @ flower-like ZnO microspheres, Au nanorods @ normal ZnO spheres (Au–ZnO-n) were prepared in the same way and were named as Au–ZnO-n.

Characterization methods

For X-ray diffraction patterns (XRD), HZG41B-PC (Japan) and Cu-K irradiation were used to analyze the crystal structure and lattice parameters of the catalysts. For morphological study of catalysts, field emission scanning electron microscopy (FESEM) was observed by Hitachi S-4800 (Japan). Transmission electron microscopy (TEM) was conducted by JEOL JEM-2100F (Japan). X-ray photoelectron spectroscopy (XPS) measurement was recorded by VG ESCALAB 210 electron spectrometer (UK). Element contents were determined by atomic absorption spectrometer (AAS) and PANalytical Epsilon3-XL (Netherlands) X-ray fluorescence (XRF). The UV–Vis absorbance and diffuse reflectance spectra were revealed by PerkinElmer Lambda 750 S (USA). The photoluminescence (PL) was performed by Renishaw InVia Reflex laser Raman spectrometer (UK) using 325-nm He-Cd light source.

Photocatalytic activity tests

The photocatalytic performance of flower-like ZnO, different Au nanorods @ flower-like ZnO, Au nanorods @ normal ZnO and pure ZnO spheres was estimated by photodegradation of RhB (1 mg/L). 100 mg of photocatalysts was added into 200 mL of solution in a quartz beaker. The mixture was first kept in the dark condition for 0.5 h under magnetic stirring. The initial pH of RhB solution was 4.76, without adjustment during the photocatalysis process. Afterward, a 300-W Xenon lamp equipped was used as a visible light source (420–780 nm). At every interval time, the UV–Vis spectra of RhB solution were measured, and the absorbance at 553 nm was used to estimate the RhB concentration. Agilent 1260

Table 1 Au weight percentage content in Au–ZnO spheres

Sample	Au–ZnO-0.1	Au–ZnO-0.5	Au–ZnO-1	Au–ZnO-2	Au–ZnO-3	Au–ZnO-4	Au–ZnO-n
Au weight percentage content (%)	0.112	0.501	1.020	1.791	2.476	3.879	0.514

High-Performance Liquid Chromatography (HPLC, USA) and Agilent 6410 Liquid Chromatography Mass Spectrometer (LC–MS, USA) were also employed to identify the degradation intermediates of RhB.

Photoelectrochemical measurements

The electrochemical impedance spectroscopy (EIS) was carried out using a standard three-electrode cell. A platinum piece and Ag/AgCl were used as counter electrodes and reference electrode. 200 mL of Na_2SO_4 solution (0.1 M) was used as the electrolyte by an electrochemical workstation (CHI 660 E, Shanghai Chenhua, China).

Results and discussion

Structure characterization

XRD patterns analysis

The XRD pattern results of the flower-like ZnO microspheres (ZnO), normal ZnO (ZnO-n), Au–ZnO and Au–ZnO-n particles are shown in Fig. 1. For flower-like ZnO microspheres (ZnO) and normal ZnO particles (ZnO-n), the same diffraction peaks of ZnO have been detected, in which the peaks at 31.8°, 34.5°, 36.7°, 47.6°, 56.6°, 62.9°, 68.0° and 69.0° are corresponding to the (100), (002), (101), (102), (110), (103), (112) and (201) crystal planes of ZnO, according to the JCPDS standard of No. 36-1451. Furthermore, no characteristic impurity peaks were observed in the two XRD patterns, implying the high purity of the ZnO products. The diffraction peaks at 38° which is corresponding to the (111) crystal planes of Au according to the JCPDS standard of No. 04-0784 had been detected in both Au–ZnO and Au–ZnO-n proving the existence of metallic Au in the two kinds of Au–ZnO microspheres. Moreover, no shift of diffraction peaks is observed, indicating that the Au has been successfully loaded on the surface of the ZnO instead of replacing Au into ZnO crystal lattice or Au interstitial of atom [25].

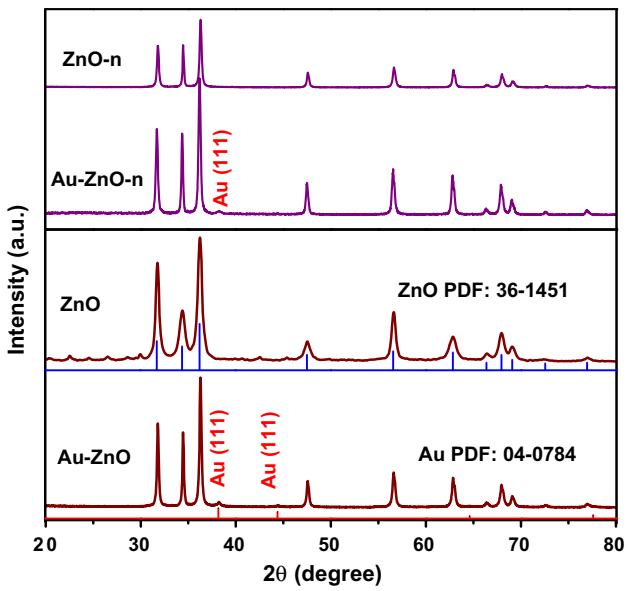

Figure 1 X-ray diffraction (XRD) patterns of pure flower-like ZnO spheres (ZnO), Au nanorods–ZnO spheres (Au–ZnO), pure normal ZnO particles (ZnO-n) and Au nanorods–normal ZnO (Au–ZnO-n).

XPS and XRF analysis

The typical survey XPS spectrum of pure flower-like ZnO and Au–ZnO is shown in Fig. 2. As shown in Fig. 2b, the Zn 2*p* consists of two peaks 1021.2 and 1044.1 eV corresponding to the Zn $2p_{3/2}$ and $2p_{1/2}$ for pure flower-like ZnO. However, Fig. 2b shows the binding energy of the Zn 2*p* ($2p_{3/2}$ and $2p_{1/2}$) for the Au–ZnO spheres was 1020.6 and 1043.7 eV which were shifted to the lower binding energy compared with the corresponding value of the pure flower-like ZnO spheres. This phenomenon is due to the interaction between Au and ZnO [38]. The O 1*s* spectra are analyzed in Fig. 2c. As shown in Fig. 2c, the O 1*s* signals of ZnO and Au–ZnO could be divided into two peaks. The binding energy of 530.0 and 529.2 eV can be attributed to the Zn–O binding for pure flower-like ZnO and Au–ZnO, respectively. The other binding energy of 531.4 and 530.5 eV might be attributive to the Zn-OH or O^{2-} ions in oxygen-deficient regions for pure flower-like ZnO and Au–ZnO, respectively [25]. The same binding energy of O 1*s* for Au–ZnO was shifted to the lower binding energy compared with the corresponding value of the pure flower-like ZnO, which further confirmed the interaction between Au and ZnO. The Au $4f_{7/2}$ and $4f_{5/2}$ can be found at binding energy of 82.5 and 87.6 eV in Au–ZnO spheres, respectively (Fig. 2d). In addition to that, the peak of Zn $3p_{1/2}$ is shown in Fig. 2d which partially overlaps with that of Au $4f_{5/2}$. This phenomenon is due to the low content of Au in the Au–ZnO, and the phenomenon can also prove that Au

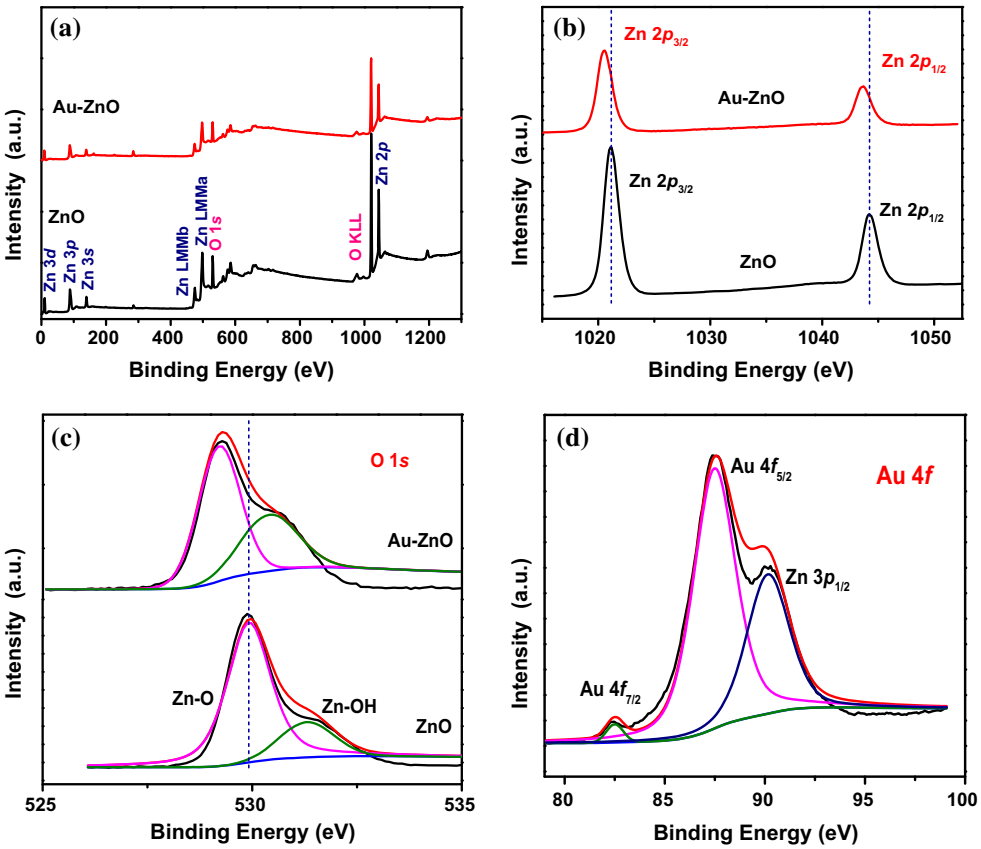

Figure 2 XPS spectrum of flower-like ZnO and Au–ZnO spheres: **a** full spectrum, **b** fine scan of Zn 2*p*, **c** fine scan of O 1s, **d** fine scan of Au 4*f*.

has been successfully loaded on the surface of the ZnO.

To quantify the content of Au in different Au–ZnO particles, the percentages of Au were determined by X-ray fluorescence (XRF) and atomic absorption spectrometer (AAS). As shown in Table 1, by changing Au concentration in the initial solutions, the Au contents were measured in the final composites.

Morphologic characterization

SEM, TEM and X-ray map analysis

The typical SEM images of pure flower-like ZnO spheres, Au–ZnO spheres and the normal Au–ZnO-n particles are shown in Fig. 3. Figure 3a and b shows a typical SEM image of flower-like ZnO microspheres, and the petals of the flowers were self-assembled by ZnO nanorods. The average diameter of the flower-like ZnO spheres was 2–3 μm. As shown in Fig. 3c, Au–ZnO retained the flower-like nanostructure of ZnO spheres. The SEM image of Au–normal ZnO (Au–ZnO-n) is shown in Fig. 3d. Figure 3e shows back-scattered electron image of the Au–ZnO, in which the bright spot was Au nanorods. In order to further confirm the existence of Au nanorods, elemental mapping is used in Fig. 3f–h. It can be clearly observed that the O, Au and Zn had uniform distribution in the flower-like ZnO spheres.

Figure 4 displays the typical TEM images of Au–ZnO, and the Au nanorods were loaded on the surface of ZnO spheres (Fig. 4b, c). The Au nanorods have a length of about 45 nm and a width of about 13 nm (Fig. 4a, inset figures are length and width distribution figures of Au nanorods). The HRTEM image (Fig. 4d) shows that the lattice fringes corresponded to crystalline Au nanorods and flower-like ZnO microspheres, respectively. The interplanar distances of 0.235 and 0.191 nm agreed well with the (111) crystal planes of Au nanorods and the (102) crystal planes of flower-like ZnO microspheres, respectively. Interestingly, the cross-fringes could be observed in the interface between Au nanorods and ZnO, revealing the in situ deposited of Au nanorods onto flower-like ZnO microspheres.

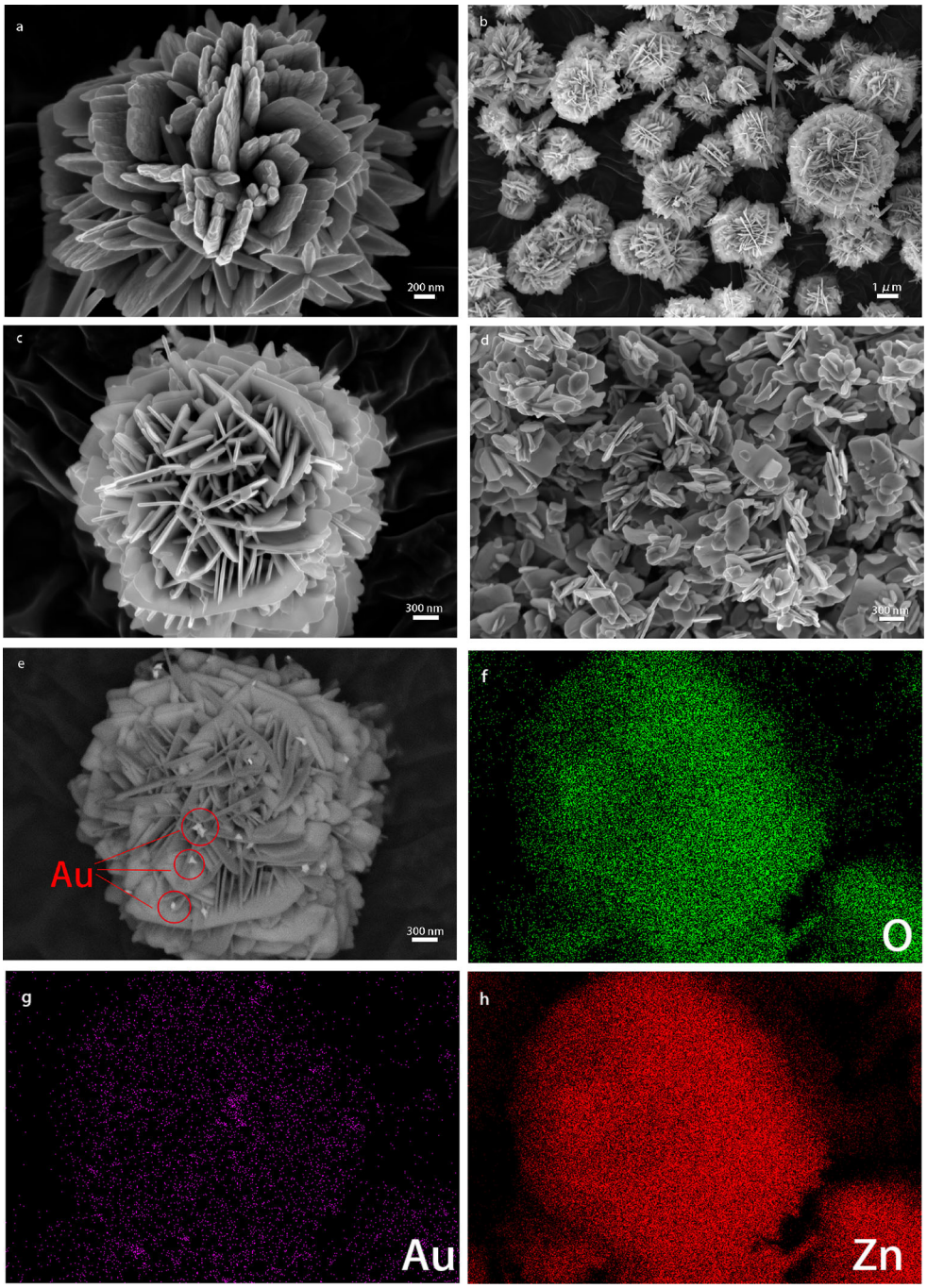

Figure 3 **a**, **b** SEM images of flower-like ZnO spheres, **c** SEM image of Au–ZnO-0.5 spheres, **d** SEM image of Au nanorods–normal ZnO (Au–ZnO-n) particles, **e** ESB image of Au–ZnO-0.5 spheres, **f** the elemental mappings of O, **g** the elemental mappings of Au, **h** the elemental mappings of Zn in Au–ZnO-0.5 spheres.

The optical properties

UV–Vis DRS analysis

The UV–Vis diffuse reflectance spectra results of Au nanorods and flower-like ZnO microspheres with different amounts of Au loading are shown in Fig. 5. The absorption band peak of pure ZnO spheres is at around 370 nm, and in contrast, the absorption band peak of Au nanorods is at around 580 nm which is higher than the absorption peak of 550 nm for Au nanospheres reported in the literature [25]. This phenomenon has been reported by El-Sayed [27] and

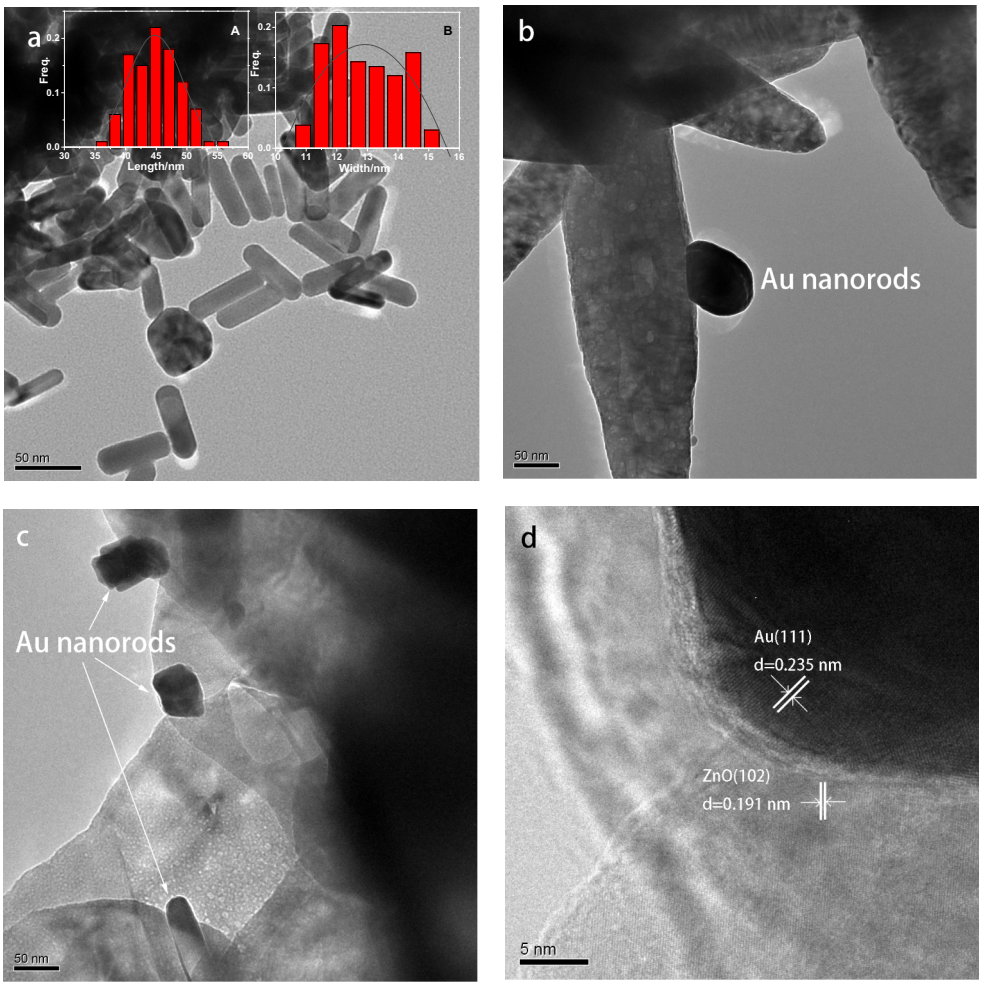

Figure 4 TEM image of **a** Au nanorods (inset is length and width distribution figures of Au nanorods), **b**, **c** Au–ZnO spheres, **d** HRTEM image of Au–ZnO spheres.

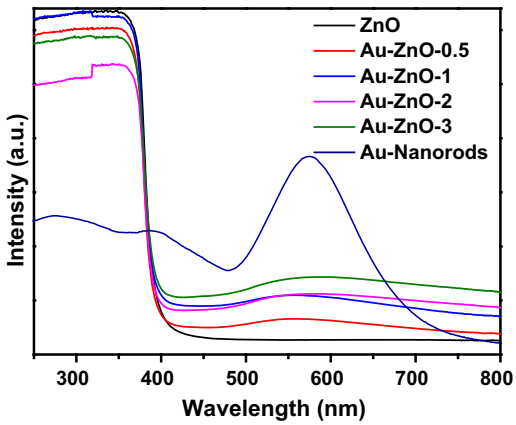

Figure 5 UV-visible absorption spectra of ZnO spheres, Au–ZnO-0.5, Au–ZnO-1, Au–ZnO-2, Au–ZnO-3 spheres and Au nanorods.

Jianfang Wang [39], by adjusting the shape of Au nanoparticles from nanospheres to nanorods, not only can change absorption band and occur in red-shift, from visible to NIR region, but also can enhance their absorption. As for Au nanorods, there is the transverse LSPR mode which is excited by light polarized along the transverse direction of the nanorods, as well as the longitudinal LSPR mode which is associated with the electron oscillations along the length axis [40]. The plasmon wavelength is produced from the longitudinal LSPR mode which can be synthetically tuned across a broad spectral range, covering the visible and near-infrared regions by tailoring their length and diameter [23]. Due to the surface plasmon resonance effect (SPR) of Au nanorods, the Au-loaded ZnO crystals display an obvious additional visible light absorption band. For Au–ZnO spheres, the visible light absorption

spectrum is much wider and weaker than the pure Au due to the SPR effect. When Au nanorods were loaded into ZnO, the plasmon resonances of the Au nanorods can enhance the light absorption in the adjacent ZnO, then further the dielectric constant would be affected and the intensity of SPR peaks would obviously be effected; therefore, the absorption band peak of Au–ZnO spheres is seen between 500 and 700 nm in Fig. 5. This phenomenon is conducive to the use of visible light for photocatalysts, thereby enhancing the photocatalytic effect.

PL spectra analysis

To study the recombination of electrons and holes in Au–ZnO spheres, the photoluminescence spectra (PL) were used. The result is shown in Fig. 6. Compared with pure flower-like ZnO microspheres, the different Au–ZnO compounds show lower emission intensity which indicated that the recombination of the photogenerated electron–hole pairs was significantly suppressed after the Au nanorods formed on the surface of the flower-like ZnO microspheres. This phenomenon is attributed to the efficient charge transfer between Au nanorods and flower-like ZnO microspheres. Interestingly, with the increasing in the amount of Au load, the emission intensity first decreased and then increased. Significantly, Au–ZnO-0.5 exhibited the lowest emission intensity which could be attributed to the SPR effect of Au nanorods on the surfaces of flower-like ZnO microspheres. Obviously, the Au nanorods remarkably capture photogenerated electrons, which can effectively suppress photogenerated electron–holes recombination. When the Au content is too high, the Au nanorods will form a recombination center of electron–holes and will promote the recombination of electrons and holes; therefore, the emission intensity will increase.

Photoelectrochemical performance

The photocatalytic activity of semiconductors mainly depends on the photogenerated charge interface separation. The separation and transmission efficiency of electrons and holes in the semiconductors are important index to evaluate the performance of photocatalytic materials. The photoelectrochemical performance such as electrochemical impedance spectroscopy (EIS) is a good analytical method to detect the efficiency of photogenerated charge interface separation. Figure 7 shows the EIS Nuquist plots of electrode for pure flower-like ZnO microspheres, Au–ZnO-0.1, Au–ZnO-0.5, Au–ZnO-1, Au–ZnO-2 and Au–ZnO-n. The arc radius on the EIS Nyquist plot reveals the interface layer resistance occurred at the surface of the electrode, and the smaller arc radius implied lower resistance and higher effective interfacial charge transfer process [41]. Figure 7 shows the arc radius of Au–ZnO-0.5 was the smaller than pure ZnO. After doping with Au nanorods, the rate of photogenerated electrons captured from Au nanorods suppresses the recombination rate of electron–hole pairs. Interestingly, the arc radius of the Au–ZnO-1 and Au–ZnO-2 is larger than pure flower-like ZnO. This phenomenon is due to the excessive Au nanorods loaded, resulting in Au nanorods to

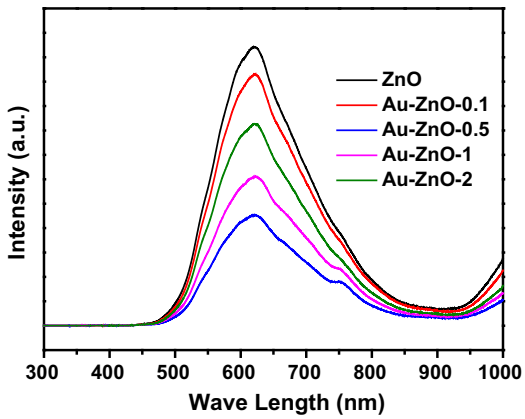

Figure 6 PL emission spectra of pure ZnO spheres, Au–ZnO-0.1, Au–ZnO-0.5, Au–ZnO-1 and Au–ZnO-2 spheres.

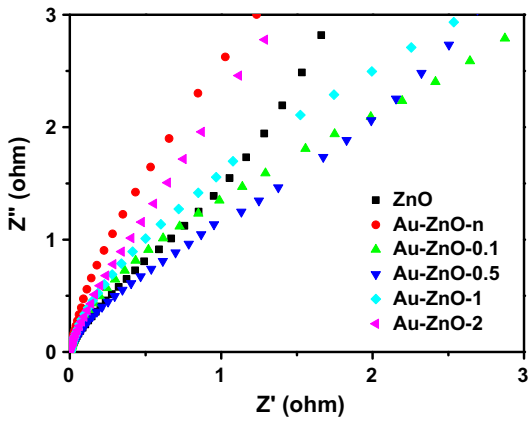

Figure 7 EIS Nyquist plots of pure flower-like ZnO spheres, Au–ZnO-0.1, Au–ZnO-0.5, Au–ZnO-1, Au–ZnO-2 spheres and Au–ZnO-n particles.

become a recombination center of electrons and holes.

Photocatalytic activity

The photocatalytic performance of photodegradation of rhodamine B (RhB) by ZnO and Au–ZnO under visible light irradiation is shown in Fig. 8. It can be seen that the RhB could be rarely degraded under visible light irradiation without photocatalysts and the pure flower-like ZnO exhibited no photoactivity because of the large energy gap (3.37 eV). Obviously, after doping with Au nanorods, Au–ZnO could absorb visible light due to the SPR effect, which leads to the degradation of RhB. It is observed that the Au–ZnO-0.5 exhibited the best photoactivity, completely destroying RhB in solution after 300 min. The optimal value of Au nanorod doping could absorb resonant photons and transfer the electrons to the CB of ZnO leading to the separation of electrons and holes. Too little Au nanorod doping may not provide enough electrons to the CB of ZnO; however, the excess Au nanorod doping may act as recombination center for electron–hole pairs. Interestingly, Au–ZnO-n exhibited the worst photoactivity. This phenomenon is due to the unique structure of the flower-like ZnO which facilitates the adsorption of the dye molecules on the catalyst surface, while more dissolved oxygen and water reach to the surface of the catalyst, resulting in more radicals for RhB degradation [42]. This step is essential for the photocatalysis. Moreover, the flower-like morphology is more likely

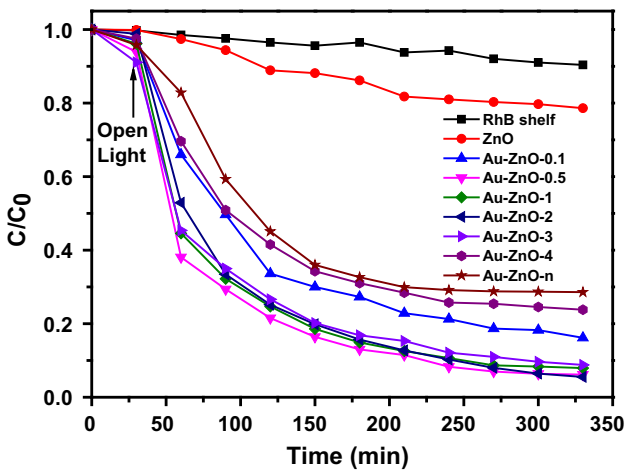

Figure 8 Photocatalytic activities of ZnO, Au–ZnO-0.1, Au–ZnO-0.5, Au–ZnO-1, Au–ZnO-2, Au–ZnO-3, Au–ZnO-4 spheres and Au–ZnO-n particles for the degradation of RhB.

to absorb visible light and enhance the photocatalytic efficiency.

The stability of photocatalytic materials is very important for the industrial application. For this reason, the stability of photocatalytic materials has been investigated. As shown in Fig. 9, after five cycling tests, the degradation efficiency of RhB did not show any significant change, indicating that the as-prepared Au–ZnO spheres were stable and effective for degradation of organic dyes in water under visible light irradiation.

Photocatalytic degradation mechanism

In general, in the process of photocatalytic oxidation degradation of dye, the main active species are holes, superoxide radicals and hydroxyl radical [34]. It is important to infer the reaction mechanism through determination of active species involved in photocatalytic reactions. In this study, several different scavengers such as potassium iodide (KI), N_2 bubble and isopropanol (Isop) were selected to quench h^+, $^{\cdot}O^{2-}$ and $^{\cdot}OH$ formed during the degradation of RhB. As shown in Fig. 10, the reaction rate of photocatalytic oxidation degradation of RhB was affected slightly by isopropanol and KI addition, indicating that the $^{\cdot}OH$ and h^+ species played little role in the reaction mechanism for RhB oxidation under visible light irradiation. However, when N_2 bubble was bubbled to the RhB solution, the degradation effect has been significantly inhibited, indicating that the $^{\cdot}O^{2-}$ played an essential role in the reaction mechanism for RhB degradation.

For a better understanding of the reaction pathway of RhB, the temporal adsorption UV spectral changes of the RhB solution during UV light irradiation and visible light irradiation were analyzed and the results are shown in Fig. 11a and b. Figure 10a shows when irradiated by UV light, RhB gradually degraded in the flower-like ZnO microspheres system; however, maximum adsorption peak of the RhB (553 nm) had a slightly movement. On the contrary, when irradiated by visible light, the absorption peak undergoes a decrease with a hypsochromic shift from 553 to 520 nm (Fig. 11b). It has been reported in the literature, when the hypsochromic shifts of the RhB absorption occurred in photocatalytic reactions due to the *N*-deethylation of RhB [43, 44], however, when the hypsochromic was not obvious, the reaction pathway of RhB degradation might be a direct

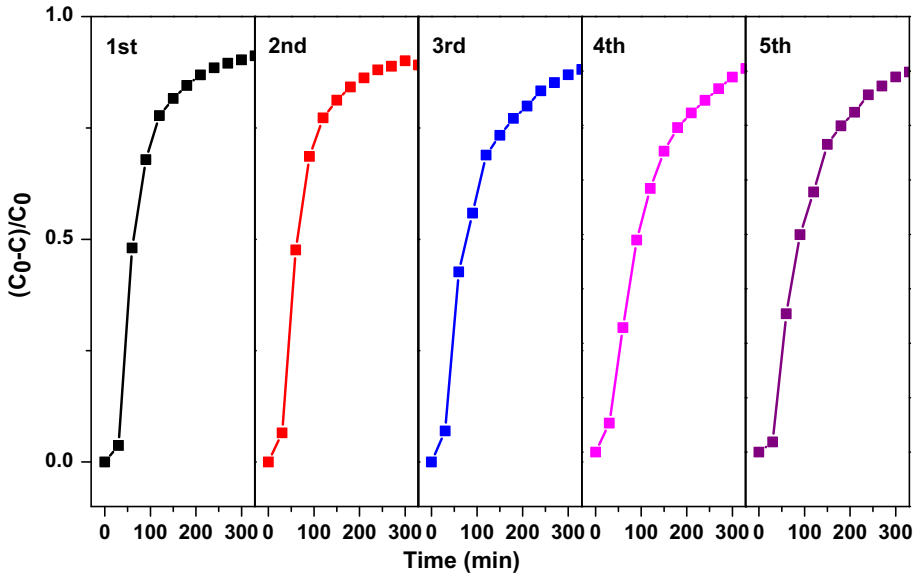

Figure 9 Photocatalytic activities of Au–ZnO-0.5 spheres during the recycling experiments.

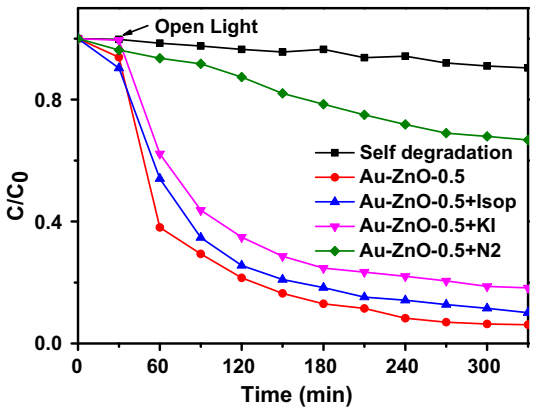

Figure 10 Effects of different scavenger addition in the photocatalytic degradation of RhB under visible light irrigation.

cleavage of the chromophore structure [34]. It is concluded that the degradation of RhB under visible light by Au–ZnO spheres was mainly due to the cleavage of the *N*-deethylation of RhB because of obviously deethylation (Fig. 11).

In order to further clarify the degradation mechanism of RhB by Au–ZnO under visible light irradiation, LC coupled with MS was used to detect the intermediates generated during the RhB degradation process. The HPLC results of the original RhB and the intermediate products of each 30 min until 300-min visible light irradiation are shown in Fig. 12.

Figure 12 shows that the retention time of RhB solution was 16.29 and 11.16 min at the beginning, the m/z value of which was 443.4 and 415.3, respectively. When irritated by the visible light, the peak

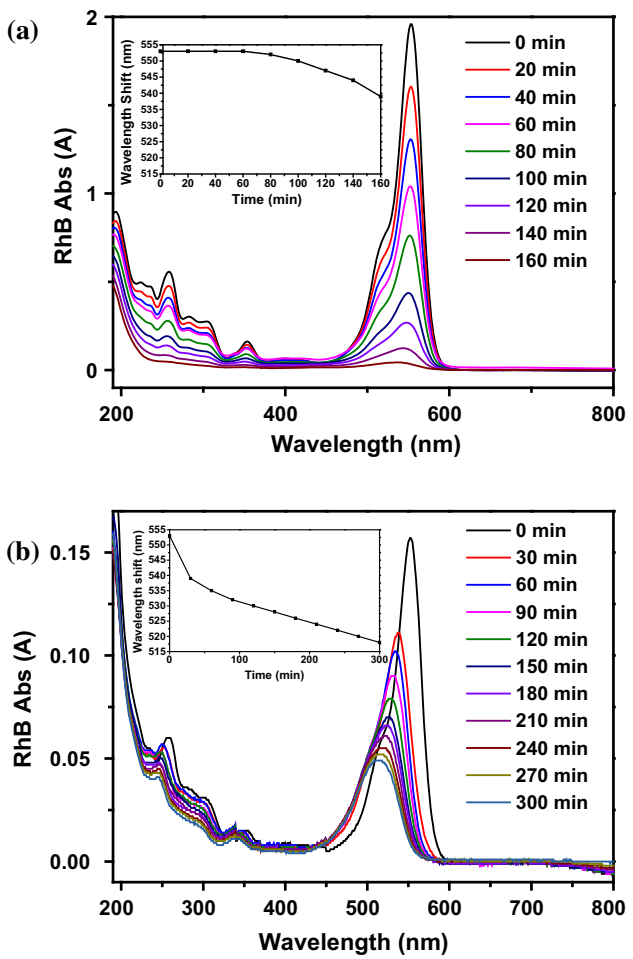

Figure 11 UV-visible adsorption spectral changes for the RhB solution **a** ZnO (under UV–Vis light), **b** Au–ZnO spheres (under visible light).

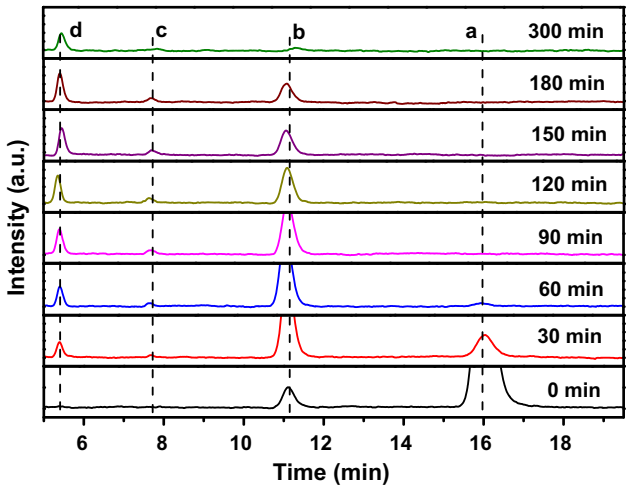

Figure 12 HPLC chromatograms of the *N*-deethylated intermediates recorded at 550 nm at 0, 30, 60, 90, 120, 150, 180 and 300 min.

area of the peak with the retention time of 16.29 min began to decrease and the peak area of the peak with the retention time of 11.16 min began to rise; in the meantime, the peaks with retention time of 7.82 and 5.49 min appeared, the m/z value of which was 387.3 and 359.3. With the increasing of reaction time, the peak area of m/z 443.4 gradually declined and the peak area of m/z 415.3, 387.3 and 359.3 was increased at first and then decreased. It is evident that the value of 443.4, 415.3, 387.3 and 359.3 gradually lost 28 m/z which are the value of an ethyl group. According to the relevant literature reported and combining with MS analysis, the mass peaks at m/z 443.4, 415.3, 387.3 and 359.3 were identified as RhB and its *N*-deethylated intermediates which were named, N,N,N′-triethyl rhodamine (DER), N, N-diethylrhodamine (DR), N-ethyl-N-ethylrhodamine (EER) and N-ethyl rhodamine (ER) [45]. Among them, DR and EER are a pair of isomers [46]. Moreover, by the percentage of the degradation products in the HPLC, we can deduce the degradation process of RhB. In the original RhB solution, the percentage of RhB was 93.9% and the percentage of DER was 6.1%. After 30-min visible light irradiation, the percentage of RhB was reduced to 24.3%, the percentage of DER was increased to 67.9% and DR, and EER and ER began to appear with the 3.5, 3.5 and 0.8% percentage, respectively. When the irradiation time increased to 90 min, the peak of RhB completely disappeared, and the percentage of DER, DR, EER and ER was 76.3, 9.8, 9.7 and 4.2%. This phenomenon illustrated that the degradation mechanism of RhB by Au–ZnO under visible light was mainly the process of deethylation from RhB (443.4 m/z) to DER (415.3 m/z), DR (387.3 m/z) or EER (387.3 m/z), and ER (359.3 m/z) [42], which correspond to the UV spectral results.

We deduced the mechanism of photocatalytic degradation of RhB by Au–ZnO flower-like microspheres. First, RhB and oxygen in the water reached to the vicinity of Au–ZnO, and due to the unique flower-like structure of Au–ZnO, they were adsorbed on the surface by a hydrogen bonding interaction between carboxyl groups of RhB and surface hydroxyl groups of photocatalyst. This process lasted nearly 30 min until the adsorption equilibrium was reached.

Secondly, the system was photon-activated by visible light; the Au nanorods @ flower-like ZnO microspheres began to absorb visible light due to the SPR effect. When the light wave passes through Au–ZnO spheres, the Au nanorod electron density was polarized to one side and oscillates in resonance with the light frequency and a metal–semiconductor Schottky barrier was formed due to the lower Femi level of ZnO when compared to metallic Au [20]. And then Au nanorods continue to absorb the resonant photons and the photogenerated electrons transfer from excited Au nanorods to CB of flower-like ZnO microspheres which would promote the separation of electron–holes and also would help the reduction in the recombination probability of formed election–holes, as shown in Scheme 1.

Thirdly, the photogenerated electrons in Au nanorods and those transferred to the ZnO spheres

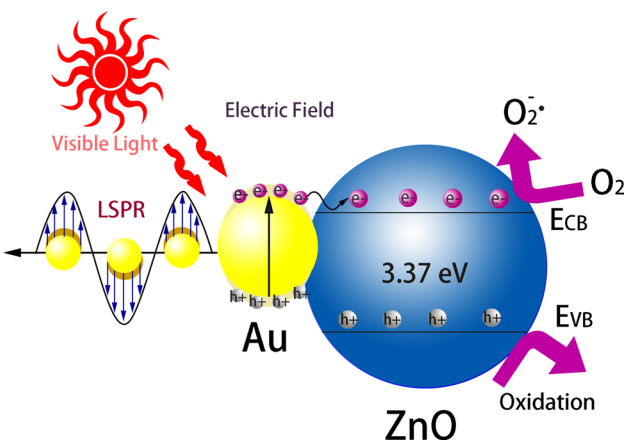

Scheme 1 Schematic diagram showing the enhanced photocatalytic activity of the Au–ZnO flower-like spheres under visible light irradiation.

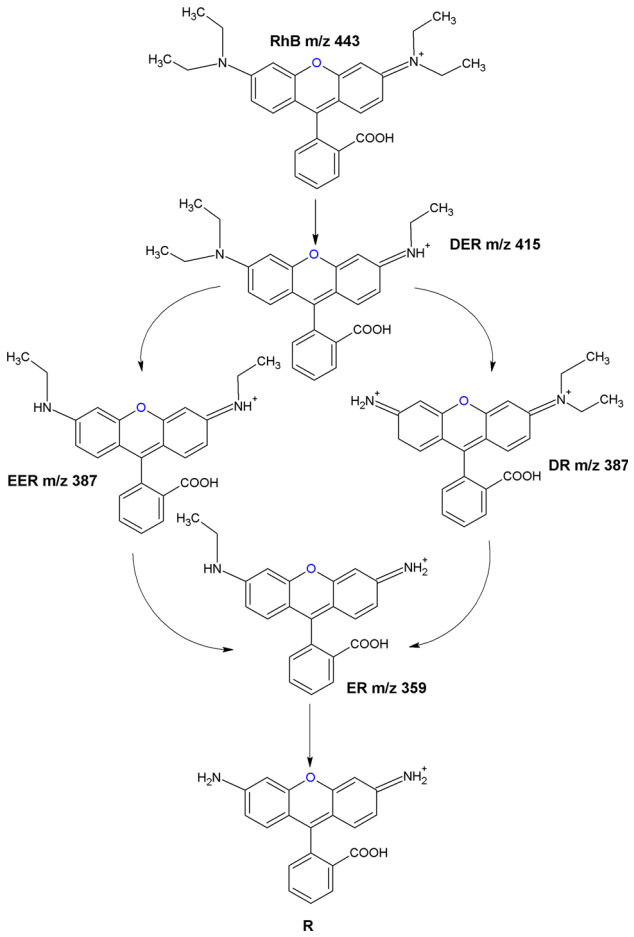

Scheme 2 Schematic diagram showing proposed photocatalytic mechanism of RhB solution under visible light irradiation.

could be trapped by O_2 to from $\cdot O^{2-}$ and the N-ethyl group of RhB was first attacked by $\cdot O^{2-}$ to form DER (415.3 m/z); with the continuous attack of $\cdot O^{2-}$, the DER was further *N*-deethylated into DR and EER and then into ER. After *N*-deethylation, the reaction composes became more complex and the opening ring process began with the formation of oxides and small molecule compounds. After that the formed oxidized intermediates were further mineralized into CO_2, NO_3^-, NH_4^+ and H_2O [47], as shown in Scheme 2.

Conclusions

In this study, we have demonstrated that flower-like ZnO microspheres could be successfully fabricated via a solvothermal method and Au nanorods were loaded on the surface of flower-like ZnO microspheres. The new structure of Au nanorods @ flower-like ZnO microspheres was confirmed to exhibit significant photodegradation activity on RhB under visible light. The enhanced photocatalytic performance was attributive to the flower-like structure of ZnO microspheres and the Au nanorod loading. The flower-like structure of ZnO microspheres was demonstrated to facilitate the adsorption of the dye molecules and dissolved oxygen on the surface of the catalyst. Moreover, the Au nanorods could absorb visible light to form SPR effect which made the electrons from Au transfer to the CB of ZnO and thus facilitates the separation of electron and holes. Superoxide radicals ($\cdot O^{2-}$) played a major role in the photocatalytic degradation of RhB leading to *N*-deethylated of RhB. The different effect of Au nanorod loading on photocatalysis was also studied and the Au–ZnO-0.5 exhibited the best photoactivity. This work provides a new method for low Au nanorod-supported photocatalyst that has an efficiently degradation of organic dyes containing wastewater under visible light.

Acknowledgements

This work was partially supported by the National Natural Science Foundation of China (21277108).

References

[1] Bumajdad A, Madkour M, Abdel-Moneam Y, El-Kemary M (2014) Nanostructured mesoporous Au/TiO2 for photocatalytic degradation of a textile dye: the effect of size similarity of the deposited Au with that of TiO2 pores. J Mater Sci 49:1743–1754. https://doi.org/10.1007/s10853-013-7861-0

[2] Fujishima A, Honda K (1972) Electrochemical Photolysis of Water at a Semiconductor Electrode. Nature 238:37–38

[3] Du P, Song L, Xiong J, Cao H (2013) Photocatalytic degradation of Rhodamine B using electrospun TiO2 and ZnO nanofibers: a comparative study. J Mater Sci 48:8386–8392. https://doi.org/10.1007/s10853-013-7649-2

[4] Sakthivel S, Neppolian B, Shankar MV, Arabindoo B, Palanichamy M, Murugesan V (2003) Solar photocatalytic degradation of azo dye: comparison of photocatalytic efficiency of ZnO and TiO2. Sol Energy Mater Sol Cells 77:65–82

[5] Sivula K, Le Formal F, Graetzel M (2011) Solar Water Splitting: progress Using Hematite (alpha-Fe2O3) Photoelectrodes. Chemsuschem 4:432–449

[6] Balachandran S, Swaminathan M (2012) Facile Fabrication of Heterostructured Bi2O3-ZnO Photocatalyst and Its Enhanced Photocatalytic Activity. J Phys Chem C 116:26306–26312

[7] Yan SC, Li ZS, Zou ZG (2009) Photodegradation Performance of g-C3N4 Fabricated by Directly Heating Melamine. Langmuir 25:10397–10401

[8] Gomez JL, Tigli O (2013) Zinc oxide nanostructures: from growth to application. J Mater Sci 48:612–624. https://doi.org/10.1007/s10853-012-6938-5

[9] Georgekutty R, Seery MK, Pillai SC (2008) A highly efficient Ag-ZnO photocatalyst: synthesis, properties, and mechanism. J Phys Chem C 112:13563–13570

[10] Chen D, Wang K, Ren T, Ding H, Zhu Y (2014) Synthesis and characterization of the ZnO/mpg-C3N4 heterojunction photocatalyst with enhanced visible light photoactivity. Dalton Trans 43:13105–13114

[11] Zou X, Fan H, Tian Y, Yan S (2014) Synthesis of Cu2O/ZnO hetero-nanorod arrays with enhanced visible light-driven photocatalytic activity. CrystEngComm 16:1149–1156

[12] Xu F, Yuan Y, Han H, Wu D, Gao Z, Jiang K (2012) Synthesis of ZnO/CdS hierarchical heterostructure with enhanced photocatalytic efficiency under nature sunlight. CrystEngComm 14:3615–3622

[13] Zong X, Sun C, Yu H et al (2013) Activation of Photocatalytic Water Oxidation on N-Doped ZnO Bundle-like Nanoparticles under Visible Light. J Phys Chem C 117:4937–4942

[14] Sun S, Chang X, Li X, Li Z (2013) Synthesis of N-doped ZnO nanoparticles with improved photocatalytical activity. Ceram Int 39:5197–5203

[15] Zhu Y-P, Li M, Liu Y-L, Ren T-Z, Yuan Z-Y (2014) Carbon-Doped ZnO Hybridized Homogeneously with Graphitic Carbon Nitride Nanocomposites for Photocatalysis. J Phys Chem C 118:10963–10971

[16] Liu S, Li C, Yu J, Xiang Q (2011) Improved visible-light photocatalytic activity of porous carbon self-doped ZnO nanosheet-assembled flowers. CrystEngComm 13:2533–2541

[17] Zhao L, Chen X, Wang X et al (2010) One-Step Solvothermal Synthesis of a Carbon@TiO2 Dyade Structure Effectively Promoting Visible-Light Photocatalysis. Adv Mater 22:3317–3321

[18] Zhang D, Zeng F (2012) Visible light-activated cadmium-doped ZnO nanostructured photocatalyst for the treatment of methylene blue dye. J Mater Sci 47:2155–2161. https://doi.org/10.1007/s10853-011-6016-4

[19] Xu C, Cao L, Su G, Liu W, Qu X, Yu Y (2010) Preparation, characterization and photocatalytic activity of Co-doped ZnO powders. J. Alloys Compd. 497:373–376

[20] Bumajdad A, Madkour M (2014) Understanding the superior photocatalytic activity of noble metals modified titania under UV and visible light irradiation. Phys Chem Chem Phys 16:7146–7158

[21] She P, Xu K, He Q, Zeng S, Sun H, Liu Z (2017) Controlled preparation and visible light photocatalytic activities of corn cob-like Au–ZnO nanorods. J Mater Sci 52:3478–3489. https://doi.org/10.1007/s10853-016-0639-4

[22] Alammar T, Mudring A-V (2009) Facile preparation of Ag/ZnO nanoparticles via photoreduction. J Mater Sci 44:3218–3222. https://doi.org/10.1007/s10853-009-3429-4

[23] Chen H, Shao L, Li Q, Wang J (2013) Gold nanorods and their plasmonic properties. Chem Soc Rev 42:2679–2724

[24] Huang X, Neretina S, El-Sayed MA (2009) Gold Nanorods: from Synthesis and Properties to Biological and Biomedical Applications. Adv Mater 21:4880–4910

[25] Liu T, Chen W, Hua Y, Liu X (2017) Au/ZnO nanoarchitectures with Au as both supporter and antenna of visible-light. Appl Surf Sci 392:616–623

[26] Baffou G, Quidant R, Girard C (2009) Heat generation in plasmonic nanostructures: influence of morphology. Appl Phys Lett 94:30

[27] Huang XH, El-Sayed IH, Qian W, El-Sayed MA (2006) Cancer cell imaging and photothermal therapy in the near-infrared region by using gold nanorods. JACS 128:2115–2120

[28] Kumar SG, Rao KSRK (2015) Zinc oxide based photocatalysis: tailoring surface-bulk structure and related interfacial charge carrier dynamics for better environmental applications. Rsc Advances 5:3306–3351

[29] Xu L, Hu Y-L, Pelligra C et al (2009) ZnO with Different Morphologies Synthesized by Solvothermal Methods for Enhanced Photocatalytic Activity. Chem Mater 21:2875–2885

[30] Xie Q, Li J, Tian Q, Shi R (2012) Template-free synthesis of zinc citrate yolk-shell microspheres and their transformation to ZnO yolk-shell nanospheres. J Mater Chem 22:13541–13547

[31] Sun L, Shao R, Chen Z, Tang L, Dai Y, Ding J (2012) Alkali-dependent synthesis of flower-like ZnO structures with enhanced photocatalytic activity via a facile hydrothermal method. Appl Surf Sci 258:5455–5461

[32] Ahmad M, Shi Y, Nisar A et al (2011) Synthesis of hierarchical flower-like ZnO nanostructures and their functionalization by Au nanoparticles for improved photocatalytic and high performance Li-ion battery anodes. J Mater Chem 21:7723–7729

[33] Zeng H, Cai W, Liu P et al (2008) ZnO-based hollow nanoparticles by selective etching: elimination and

reconstruction of metal-semiconductor interface, improvement of blue emission and photocatalysis. ACS Nano 2:1661–1670

[34] Zhang Y, Zhou J, Cai W, Zhou J, Li Z (2017) Enhanced photocatalytic performance and degradation pathway of Rhodamine B over hierarchical double-shelled zinc nickel oxide hollow sphere heterojunction. Appl. Surf, Sci

[35] Tang G, Tian S, Zhou Z et al (2014) ZnO Micro/Nanocrystals with Tunable Exposed (0001) Facets for Enhanced Catalytic Activity on the Thermal Decomposition of Ammonium Perchlorate. J Phys Chem C 118:11833–11841

[36] Chen J-J, Deng X-R, Deng H (2013) Progress in the growth and characterization of nonpolar ZnO films. J Mater Sci 48:532–542. https://doi.org/10.1007/s10853-012-6721-7

[37] Sau TK, Murphy CJ (2004) Seeded high yield synthesis of short Au nanorods in aqueous solution. Langmuir 20:6414–6420

[38] Ansari SA, Khan MM, Ansari MO, Lee J, Cho MH (2013) Biogenic Synthesis, Photocatalytic, and Photoelectrochemical Performance of Ag-ZnO Nanocomposite. J Phys Chem C 117:27023–27030

[39] Jiang R, Cheng S, Shao L, Ruan Q, Wang J (2013) Mass-Based Photothermal Comparison Among Gold Nanocrystals, PbS Nanocrystals, Organic Dyes, and Carbon Black. J Phys Chem C 117:8909–8915

[40] Perez-Juste J, Pastoriza-Santos I, Liz-Marzan LM, Mulvaney P (2005) Gold nanorods: synthesis, characterization and applications. Coord Chem Rev 249:1870–1901

[41] Deng Q, Tang H, Liu G et al (2015) The fabrication and photocatalytic performances of flower-like Ag nanoparticles/ZnO nanosheets-assembled microspheres. Appl Surf Sci 331:50–57

[42] Wang XT, Zhu MY, Sun YB et al (2016) A New Insight of the Photothermal Effect on the Highly Efficient Visible-Light-Driven Photocatalytic Performance of Novel-Designed TiO2 Rambutan-Like Microspheres Decorated by Au Nanorods. Part. Part. Syst. Char. 33:140–149

[43] Watanabe T, Takizawa T, Honda K (1977) Photocatalysis through excitation of adsorbates. 1. Highly efficient *N*-deethylation of rhodamine B adsorbed to cadmium sulfide. J Phys Chem 81:1845–1851

[44] Takizawa T, Watanabe T, Honda K (1978) Photocatalysis through excitation of adsorbates. 2. A comparative study of Rhodamine B and methylene blue on cadmium sulfide. J Phys Chem 82:1391–1396

[45] Yu K, Yang S, He H, Sun C, Gu C, Ju Y (2009) Visible light-driven photocatalytic degradation of rhodamine B over NaBiO3: pathways and mechanism. J Phys Chem A 113:10024–10032

[46] Zhu ZX, Chen Y, Gu Y et al (2016) Catalytic degradation of recalcitrant pollutants by Fenton-like process using polyacrylonitrile-supported iron (II) phthalocyanine nanofibers: intermediates and pathway. Water Res 93:296–305

[47] Natarajan K, Natarajan TS, Bajaj HC, Tayade RJ (2011) Photocatalytic reactor based on UV-LED/TiO2 coated quartz tube for degradation of dyes. Chem Eng J 178:40–49